Cosmological forecasts from photometric measurements of the angular correlation function

F. Sobreira,[1,2] F. de Simoni,[2,3,4] R. Rosenfeld,[1,2] L. A. N. da Costa,[2,3] M. A. G. Maia,[2,3] and M. Makler[2,5]

[1]*Instituto de Física Teórica, Universidade Estadual Paulista, Rua Dr. Bento T. Ferraz, 271, São Paulo, SP 01140-070, Brazil*
[2]*Laboratório Interinstitucional de e-Astronomia- LineA, Rua Gal. José Cristino 77, Rio de Janeiro, RJ 20921-400, Brazil*
[3]*Observatório Nacional, Rua Gal. José Cristino 77, Rio de Janeiro, RJ 20921-400, Brazil*
[4]*Departamento de Física e Matemática, PURO/Universidade Federal Fluminense, Rua Recife s/n, Rio das Ostras, RJ 28890-000, Brazil*
[5]*Centro Brasileiro de Pesquisas Físicas, Rua Dr. Xavier Sigaud, 150, Rio de Janeiro, RJ 22290-180, Brazil*

(Received 19 August 2011; published 4 November 2011)

We study forecasts for the accuracy of the determination of cosmological parameters from future large-scale photometric surveys obtained using the full shape of the 2-point galaxy angular correlation function. The effects of linear redshift-space distortion, photometric redshift Gaussian errors, galaxy bias and nonlinearities in the power spectrum are included on our analysis. The Fisher information matrix is constructed with the full covariance matrix, including the correlation between nearby redshift shells arising from the photometric redshift error. We show that under some reasonable assumptions, a survey such as the imminent Dark Energy Survey should be able to constrain the dark energy equation of state parameter w and the cold dark matter density $\Omega_{\rm cdm}$ with a precision of the order of 20% and 13%, respectively, from the full shape of the angular correlation function alone. When combined with priors from other observations the precision in the determination of these parameters improve to 8% and 4%, respectively.

DOI: 10.1103/PhysRevD.84.103001 PACS numbers: 95.36.+x, 98.65.Dx, 98.80.Es

I. INTRODUCTION

The clustering of large-scale structure of the universe is an invaluable source of information about the fundamental parameters that determine a given cosmological model. In the standard cosmological model, its origin is related to quantum fluctuations of the inflaton field during the inflationary period, and its evolution is determined by the different components of the universe that contribute to the total energy-momentum tensor, such as cold dark matter, dark energy, baryons and relativistic particles.

Until recently, cosmological constraints from galaxy distribution were obtained with spectroscopic catalogues mostly from the 2dF [1] and SDSS [2] projects. These projects raised the study of the galaxy clustering in 3D space to a new level, with a main focus on the 2-point correlation function, both in configuration and Fourier space. In particular, they resulted in the first observation of a feature in the correlation of the matter distribution, arising from the so-called baryon acoustic oscillations (BAO) that occurred at an early stage of the evolution of the universe [3].

In the near future, projects such as the WiggleZ Dark Energy Survey[1] and the Baryon Oscillation Spectroscopic Survey[2] (BOSS) will continue improving the spectroscopic catalogues. Future projects, both ground based such as BigBOSS[3] and space based such as Euclid[4] will also rely on spectroscopic measurements of objects.

In order to collect a larger number of galaxies more efficiently, there are a number of planned galaxy surveys that will estimate the galaxy redshift from broad-band photometry measurements (photometric redshift or photo-z) with the aim to measure more than hundreds of millions up to a few billions of galaxies in a larger volume compared to spectroscopic surveys. The idea is to have a trade-off between precise spectroscopic redshifts for a relatively small number of galaxies and less precise photometric redshifts for a larger number of objects. For instance, the MegaZ-LRG photometric catalogue based on the SDSS-II DR7 has become recently available [4,5]. The measurement of the angular correlation function (ACF) for a 1.5×10^6 Luminous Red Galaxies (LRG) with photometric redshifts was performed in [6], whereas their angular power spectra (APS) was measured in [5].

The Dark Energy Survey[5] (DES) is a large dedicated photometric survey that will soon start observations. It is expected to measure $\mathcal{O}$(300 million) galaxies over an area of 5000 square degrees of the southern sky using 525 nights in the Blanco 4-meter telescope in Chile. The main goal of DES is the measurement of the dark energy equation of state parameter w up to redshift $z \sim 1.4$. This measurement will be performed using four complementary methods: distances from supernovae, large-scale structure from the galaxy distribution, number count of galaxy cluster and shear from weak leasing measurements [7].

The purpose of this paper is to determine forecasts for the precision of the determination cosmological parameters from future photometric measurements of the

[1]See http://wigglez.swin.edu.au.
[2]See http://cosmology.lbl.gov/BOSS.
[3]See http://bigboss.lbl.gov.
[4]See http://sci.esa.int/euclid.
[5]See http://www.darkenergysurvey.org.

large-scale structure of the universe, such as what will be obtained by DES, using for the first time the full shape of the galaxy correlation function. The use of the angular correlation function in a given redshift shell as an observable to infer cosmological parameters can be more appropriate than the use of the spatial correlation function in the presence of errors inherent in the photometric measurements of redshifts. We use the full shape of the angular correlation function and its covariance, both at different angles and in different redshift shells, to perform a Fisher matrix analysis of the sensitivity to cosmological parameters. Hence, we do not need to assume any parametric form of the ACF, as done in an interesting recent study [8]. Also our analysis is complementary to the study of the angular power spectrum since both techniques have advantages and disadvantages. The main disadvantage of the ACF is that the covariance matrix is highly degenerate due to large correlations among different angular scales whereas for the power-spectrum errors in a given angular scale may propagate into several peaks.

In this paper we model the ACF with 6 cosmological parameters, assuming a spatially flat universe: the dark matter density parameter $\Omega_{\rm cdm}$, the baryon density parameter Ω_b, the Hubble parameter h, the primordial index of scalar perturbations n_s, the normalization of perturbations σ_8 and the equation of state parameter for dark energy w. In addition we allow for different bias between dark matter and galaxies in each of the redshift shells. We include in the modeling the effects of linear redshift-space distortion, photometric redshift Gaussian errors, galaxy bias and nonlinearities in the power spectrum. The Fisher information matrix is constructed with the full covariance matrix from the model. In particular, we take into account the correlation between nearby redshift shells arising from the photometric redshift error. We then discuss various forecasts for the cosmological parameters in different scenarios.

This paper is organized as follows. In the next section we present the model for the angular correlation function. We include the effects of nonlinearities in the power spectrum, redshift distortions from peculiar velocities of galaxies and the photo-z errors. In order to develop some intuition, we discuss in the third section how the cosmological parameters affect the ACF. Section IV is devoted to the modeling of the covariance matrix for the measurement of the ACF in different redshift shells with different angular binnings. The Fisher matrix approach is discussed in Sec. V. Our main results are presented in Secs. VI and VII provides a summary and our conclusions.

II. MODELING THE ANGULAR CORRELATION FUNCTION

The angular correlation function $\omega(\theta)$ is related to the two-point spatial correlation function $\xi^{(s)}$ in redshift space by

$$\omega(\theta) = \int_0^\infty dz_1 f(z_1) \int_0^\infty dz_2 f(z_2) \xi^{(s)}(r(z_1, z_2, \theta)). \quad (1)$$

The function $f(z)$ is determined by the selection function of the survey $\phi(z)$, the dark matter to luminous bias factor $b(z)$ and the linear growth function $D(z)$ (normalized to $D(z=0)=1$) as $f(z) = \phi(z)b(z)D(z)$. The radial comoving distance $r(z_1, z_2, \theta)$ is the distance between two galaxies at redshifts z_1 and z_2 separated by an angle θ and in a flat cosmology (which we will assume here) it is given by the relation,

$$r = \sqrt{\chi^2(z_1) + \chi^2(z_2) - 2\chi(z_1)\chi(z_2)\cos\theta}, \quad (2)$$

where $\chi(z_i)$ is the comoving distance of the object i to us (hereafter we use units with $c=1$):

$$\chi(z) = \int_0^z \frac{dz'}{H(z')} \quad (3)$$

and $H(z)$ is the usual Hubble function determined by the composition of the universe.

The redshift-space spatial correlation function $\xi^{(s)}$ corrected from the effects of redshift distortions arising from the peculiar velocities of galaxies is given by (in the plane-parallel approximation) [9,10]

$$\begin{aligned}\xi^{(s)}(r) = &\left[1 + \frac{1}{3}[\beta(z_1) + \beta(z_2)] + \frac{1}{5}\beta(z_1)\beta(z_2)\right]\xi_0(r)P_0(\mu) \\ &- \left[\frac{2}{3}[\beta(z_1) + \beta(z_2)] + \frac{4}{7}\beta(z_1)\beta(z_2)\right]\xi_2(r)P_2(\mu) \\ &+ \left[\frac{8}{35}\beta(z_1)\beta(z_2)\right]\xi_4(r)P_4(\mu). \quad (4)\end{aligned}$$

Here the $P_\ell(\mu)$ are the usual Legendre polynomials as a function of $\mu = \hat{d}\cdot\hat{r}$ (cosine of angle between the line of sight d and r) and $\beta(z) = g(z)/b(z)$ with $g(z) = d\ln D/d\ln a$. The correlation multipoles are related to the matter power-spectrum $P_m(k)$ through

$$\xi_l(r) = \frac{1}{2\pi^2}\int dk k^2 P_m(k) j_l(kr). \quad (5)$$

The selection function $\phi(z)$ is normalized such that

$$\int_0^\infty dz \phi(z) = N \quad (6)$$

where N is the total number of objects per unit solid angle of the survey. One usually slices the survey into n redshift bins i in such a way that

$$\phi(z) = \sum_i \phi_i(z), \quad (7)$$

with

$$\phi_i(z) = n(z)W_i(z), \quad (8)$$

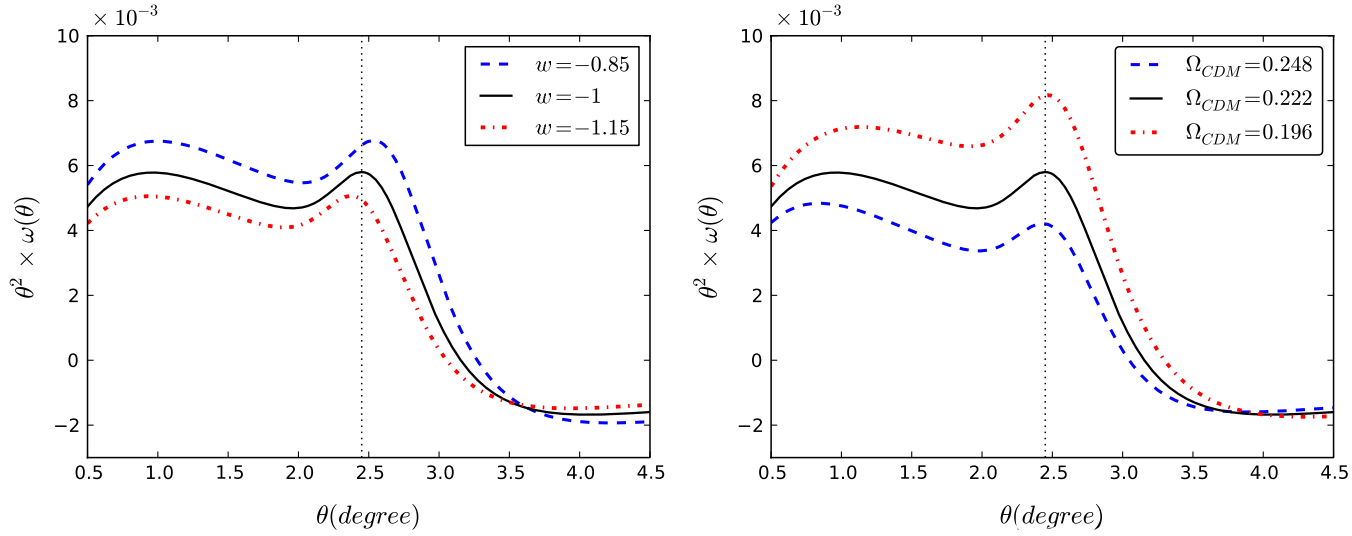

FIG. 1 (color online). Angular correlation function as a function of the angular scale for different values of the dark energy equation of state parameter w (top panel) and the cold dark matter density parameter $\Omega_{\rm cdm}$ (bottom panel) for the redshift shell $1.00 \leq z \leq 1.05$ with photo-z dispersion $\delta_\sigma = 0.03$. The vertical dotted line indicates the peak position of $\theta^2 \times \omega(\theta)$ in the fiducial cosmology as stated in the text.

where $n(z)$ is the number density of galaxies per unit solid angle and per unit redshift and $W_i(z)$ is a window function that selects the i-th redshift bin. In general, $n(z)$ is a function of the limiting magnitude of the survey. We will adopt a function of the form [11]

$$n(z) \propto (z/\bar{z})^2 e^{-(z/\bar{z})^{1.5}} \tag{9}$$

with $\bar{z} = 0.5$ being the median redshift of the survey and

$$W_i(z) = \Theta(z - z_i^{\rm low})\Theta(z_i^{\rm high} - z), \tag{10}$$

where $\Theta(x)$ is the Heaviside (or step) function.

However, in surveys where only photometric redshifts are available one should incorporate into the selection function the probability $P(z^{\rm ph}|z)$ of obtaining a true redshift z given that a photometric redshift $z^{\rm ph}$ is measured [12–15]:

$$\begin{aligned}\phi_i(z) &= n(z) \int dz^{\rm ph} W_i(z^{\rm ph}) P(z^{\rm ph}|z) \\ &= n(z) \int_{z_i^{\rm low}}^{z_i^{\rm high}} dz^{\rm ph} P(z^{\rm ph}|z).\end{aligned} \tag{11}$$

Of course in the case $P(z_{\rm ph}|z) = \delta(z_{\rm ph} - z)$, one recovers Eq. (8).

Usually the probability function for a spectroscopically calibrated galaxies is written as a gaussian distribution:

$$P_G(z^{\rm ph}|z) = \frac{1}{\sqrt{2\pi}\sigma_z} \exp\left[-\frac{(z - z^{\rm ph} - z_{\rm bias})^2}{2\sigma_z^2}\right], \tag{12}$$

with the error given by

$$\sigma_z(z) = \delta_\sigma(1 + z). \tag{13}$$

When not mentioned, we set $\delta_\sigma = 0.03$ which is expected for LRGs samples [4,16]. We will also consider here an unbiased photo-z and set $z_{\rm bias} = 0$.

Another effect that must be taken into account is the decrease in the power of the ACF due to the nonlinear gravitational clustering [17]. We will follow Crocce *et al.* [13] and model this effect phenomenologically by introducing a nonlinear power spectrum $P_{\rm NL}(k)$ and substituting (neglecting the so-called mode-coupling term):

$$P_m(k) \rightarrow P_{\rm NL}(k) = P_m(k) \exp[-r_{\rm NL}^2 k^2 D^2(z)/2] \tag{14}$$

with $r_{\rm NL} \approx 7$ Mpc h^{-1}. Even though this is a simple-minded approach, it is robust depending on the scale someone is probing. Crocce *et al.* [13] showed that this approach is in good agreement with simulations above $40h^{-1}$ Mpc, therefore our analysis will be valid and applied above this scale.

III. COSMOLOGICAL INFORMATION IN THE ANGULAR CORRELATION FUNCTION

Having a model for the angular correlation function one can study the dependencies on the cosmological parameters. The model is specified by the usual cosmological parameters. Throughout this paper we assume as fiducial cosmological model a flat ΛCDM universe with parameters as determined by WMAP7 [18]: dark matter density parameter $\Omega_{\rm cdm} = 0.222$, baryon density parameter $\Omega_b = 0.0449$, Hubble parameter $h = 0.71$, primordial index of scalar perturbations $n_s = 0.963$, and normalization of perturbations $\sigma_8 = 0.801$. In addition, we set $r_{\rm NL} = 6.6$ Mpc h^{-1}, $\delta_\sigma = 0.03$ and $b = 2$ [19].

The cosmological parameters can affect the angular correlation function in four different ways: in the primordial matter power-spectrum $P_m(k)$, the growth function $D(z)$, the linear redshift-space distortion $\beta(z)$ and in the definition of comoving distances (geometry).

The primordial power spectrum is characterized by the parameters Ω_m, Ω_b, h, n_s and σ_8 (the dark energy equation of state parameter w has a negligible impact on the primordial power spectrum in most cases). The growth function depends on Ω_m and w. The redshift space distortion parameter depends mainly on Ω_m, and the comoving distances are determined by Ω_m and w.

It is well known that there are several degeneracies among the parameters and functions, such as bias, σ_8 and the growth function. We will show below that the analysis of multiple redshift shells including redshift-space distortion can ameliorate this problem [20].

In Fig. 1 we show how the angular correlation function changes with w and $\Omega_{\rm cdm}$ around our fiducial cosmology and for the redshift shell $1.0 \leq z \leq 1.05$. From the top panel one can see that the ACF changes mostly its amplitude and the location of the BAO feature. As stated above, the primordial power spectrum does not change appreciably with w, but the growth factor $D(z)$ and the comoving distance are affected by this parameter. The contribution from the growth factor can be easily estimated. Since for this shell $D(w = -1) = 0.618$ and $D(w = -0.85) = 0.630$, the growth function can account for an increase of $\sim$3.9% in the amplitude. Hence it falls short of explaining the $\sim$14% increase of the amplitude at intermediate scales. Furthermore, the increase in $D(z)$ cannot explain the shift in the position of the BAO feature.

It is noticeable that the BAO feature shifts towards larger angular scale when going from the fiducial cosmology $w = -1$ to $w = -0.85$, while when $w = -1.15$ it shifts to smaller angular scales. The explanation comes from the fact that one changes the geometry when changing w, and distances have different values, changing the ''standard ruler.'' When converting the spatial correlation function to find the ACF, the projection depends on the thickeness of the shell in comoving distance. If the shell is wider (in comoving distance) the ACF will have less power and the projection offset will be higher. For the fiducial cosmology the thickness of the shell $1.0 \leq z \leq 1.05$ when converted to comoving distance is $\Delta\chi \simeq 87.4h^{-1}$ Mpc, while for $w = -0.85$ we have $\Delta\chi \simeq 83.6h^{-1}$ Mpc, resulting in a modification of $\sim$5% in the thickness of the comoving shell. This fact also explains why the BAO feature shifts to smaller angles from the fiducial value to $w = -0.85$ [8,21]. It is interesting that such a small change in the shell thickness can generate a non-negligible modification in the ACF shape and amplitude.

The parameter $\Omega_{\rm cdm}$ has an impact in all four effects listed above and its impact on the ACF is shown in the bottom panel of Fig. 1. However, most of the cosmological information for $\Omega_{\rm cdm}$ will come from the primordial power spectrum, with modifications in the fraction of baryons $f_b = \Omega_b/\Omega_m$ and the product $\Omega_m h$.

A complication in the simple effects illustrated above is the presence of photo-z errors, which can mimic some of the effects of changing the cosmological parameters, in addition to redshift space distortions, nonlinearities and galaxy bias. All these effects are of course taken into account in our results.

IV. MODELING THE ERRORS IN THE CALCULATION OF THE ACF

In order to derive meaningful cosmological constraints or even determine the reach of a given survey, one has to understand the errors involved in the measurements of the ACF. More precisely, one must model the full covariance matrix for measurements of the ACF at different angles and in different shells.

A. Covariance matrix for one shell

We will follow closely the works of Blake *el al.* [19] and Crocce *et al.* [13] in our modeling. The modeling will include effects from photo-z errors, redshift distortion, partial sky coverage and shot noise. For this analysis it is more convenient to work with the angular power spectrum (a derivation of the ACF covariance matrix in configuration space can be found in Cohn [22]). We define the projected density fluctuations onto the sky in a particular direction $\hat{n}$, $\sigma(\hat{n})$ as

$$\sigma(\hat{n}) = \int dz \phi(z) \delta(\hat{n}, z) \tag{15}$$

and decompose it in spherical harmonics:

$$\sigma(\hat{n}) = \sum_{l=0}^{\infty} \sum_{m=-l}^{l} a_{lm} Y_{lm}(\hat{n}). \tag{16}$$

The angular correlation function can be written as

$$\begin{aligned} \omega(\theta) &= \langle \sigma(\hat{n}) \sigma(\hat{n} + \vec{\theta}) \rangle \\ &= \left\langle \sum_{lm} \sum_{l'm'} a_{lm} a_{l'm'} Y_{lm}(\hat{n}) Y_{l'm'}(\hat{n} + \vec{\theta}) \right\rangle. \end{aligned} \tag{17}$$

From isotropy we can define C_l from

$$\langle a_{lm} a_{l'm'} \rangle = \delta_{ll'} \delta_{mm'} C_l \tag{18}$$

and therefore

$$\omega(\theta) = \sum_{lm} C_l Y_{lm}(\hat{n}) Y_{lm}(\hat{n} + \vec{\theta}) = \sum_{l} C_l \frac{2l+1}{4\pi} P_l(\cos\theta), \tag{19}$$

where the addition theorem was used in the last equality.

The C_l's are the variance of the distribution for the coefficients a_{lm}, assumed Gaussian:

$$P(a_{lm})da_{lm} = \frac{1}{\sqrt{2\pi C_l}} e^{-((a_{lm}^2)/(2C_l))} da_{lm}. \quad (20)$$

The covariance matrix is given by

$$\begin{aligned}\mathrm{Cov}\,(\omega(\theta)\omega(\theta')) &= \langle \omega(\theta)\omega(\theta')\rangle \\ &= \sum_{ll'} \mathrm{Cov}(C_l C_{l'}) \frac{2l+1}{4\pi} \\ &\quad \times \frac{2l'+1}{4\pi} P_l(\cos\theta) P_{l'}(\cos\theta'). \quad (21)\end{aligned}$$

For full sky the C_l's are statistically independent. For partial sky coverage one can use an averaged C_l over a band of width $\Delta l = 10$ and these will be independent to a good approximation. We will assume that

$$\mathrm{Cov}\,(C_l C_{l'}) = \mathrm{Var}(C_l)\delta_{ll'} \quad (22)$$

and assuming a Gaussian distribution for the likelihood function of C_l [23], correcting for partial sky coverage f_{sky} and including shot-noise error one has

$$\mathrm{Var}\,(C_l) = \frac{2}{(2l+1) f_{\mathrm{sky}}} (C_l + 1/\bar{n})^2 \quad (23)$$

where $\bar{n} = N/\Delta\Omega$ is the average number of galaxies per unit solid angle.

Therefore the covariance matrix can be computed as

$$\begin{aligned}&\mathrm{Cov}(\omega(\theta)\omega(\theta')) \\ &= \frac{2}{f_{\mathrm{sky}}} \sum_l \frac{2l+1}{(4\pi)^2} P_l(\cos\theta) P_l(\cos\theta')(C_l + 1/\bar{n})^2. \quad (24)\end{aligned}$$

We can estimate the C_l's from a model for the power spectrum by first performing a Fourier transform in the 3-d density field in Eq. (15)

$$\delta(\hat{n}, z) = \int \frac{d^3k}{(2\pi)^3} \delta(\vec{k}, z) e^{i\vec{k}\cdot\hat{n}r(z)} \quad (25)$$

and use the identity

$$e^{i\vec{k}\cdot\hat{n}r} = 4\pi \sum_{lm} i^l j_l(kr) Y_{lm}(\hat{n}) Y^*_{lm}(\hat{k}) \quad (26)$$

to compare with Eq. (16) and find

$$a^i_{lm} = \int dz \phi_i(z) \int \frac{d^3k}{(2\pi)^3} \delta(\vec{k}, z) 4\pi i^l j_l(kr) Y^*_{lm}(\hat{k}). \quad (27)$$

Defining

$$\Psi^i_l(k) = \int dz \phi_i(z) D(z) j_l(kr(z)) b(z) \quad (28)$$

with $\delta(\vec{k}, z) = D(z)\delta(\vec{k}, 0)$ allows us to write:

$$C^i_l = \langle |a^i_{lm}|^2 \rangle = \frac{2}{\pi} \int dk k^2 P_{\mathrm{NL}}(k) (\Psi^i_l)^2(k). \quad (29)$$

At this point one must also introduce the effects of redshift distortions, as done for the angular correlation function. We will adopt the prescription given in [13,24] and add to the function $\Psi_l(k)$ another term $\Psi^r_l(k)$ that incorporates the redshift distortion given by:

$$\begin{aligned}\Psi^{i,r}_l(k) = \int dz \beta(z) \phi_i(z) D(z) \Big[&\frac{2l^2+2l-1}{(2l+3)(2l-1)} j_l(kr) \\ &- \frac{l(l-1)}{(2l-1)(2l+1)} j_{l-2}(kr) \\ &- \frac{(l+1)(l+2)}{2l+1)(2l+3)} j_{l+2}(kr) \Big]. \quad (30)\end{aligned}$$

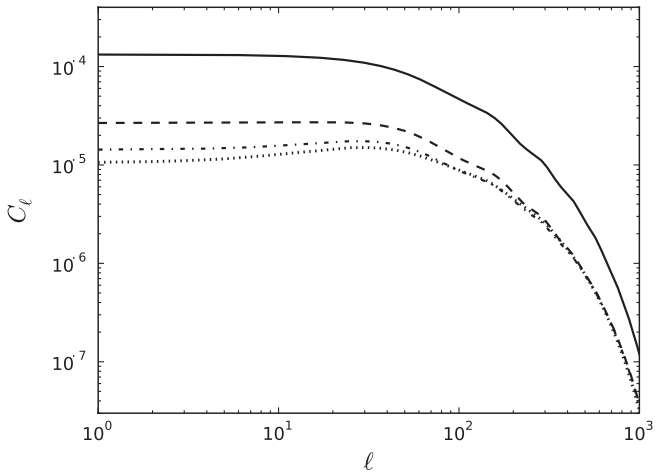

FIG. 2. Photo-z error impact on the angular power spectrum for the redshift shell $0.95 \leq z \leq 1.00$. The solid line correspond to no errors in the redshift determination, dashed line with $\delta_\sigma = 0.03$, dot-dashed line $\delta_\sigma = 0.05$ and dotted line $\delta_\sigma = 0.10$.

In Fig. 2 we show the impact of the photo-z error on the angular power spectrum for $\delta_\sigma = 0.03$, 0.05 and 0.10. One can see how the power decreases with increasing photo-z error, as expected. We also have checked the numerical agreement of the angular correlation function computed from Eq. (19) with the sum on spherical harmonics up to $l = 1000$ (to ensure numerical accuracy) with the definition given in Eq. (1).

B. Covariance matrix including different shells

The various redshift bins of the survey are not independent due to the errors in the photometric redshift. Of course the main correlations will occur for adjacent bins. Hence we need covariance matrices for 2 different redshifts i and j [19]:

$$\begin{aligned}\mathrm{Cov}\,(\omega^i(\theta_n)\omega^j(\theta_m)) &= \langle \omega^i(\theta_n)\omega^j(\theta_m)\rangle \\ &= \sum_{ll'} \mathrm{cov}(C^i_l C^j_{l'}) \frac{2l+1}{4\pi} \\ &\quad \times \frac{2l'+1}{4\pi} P_l(\cos\theta_n) P_{l'}(\cos\theta_m) \quad (31)\end{aligned}$$

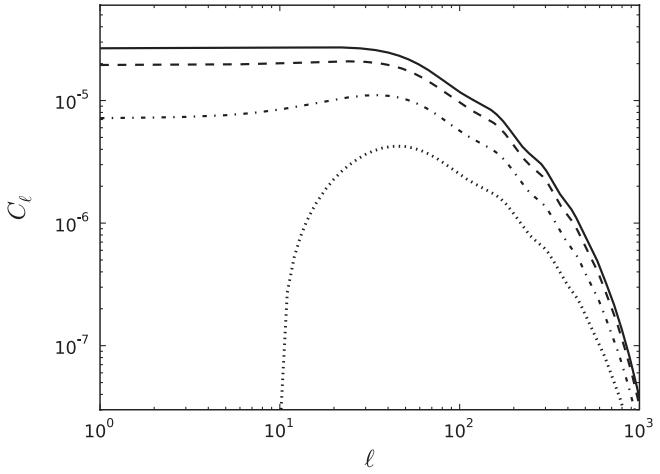

FIG. 3. Cross-correlation angular power-spectrum for the redshift shell $0.95 \leq z \leq 1.00$ with its 3 next neighbors. The solid line correspond to autocorrelation. The photo-z error was set to $\delta_\sigma = 0.03$.

where in this case, since the shot noise between shells are uncorrelated, we write

$$\mathrm{Cov}\,(C_l^i C_{l'}^j) = \frac{2}{(2l+1) f_{\mathrm{sky}}} (C_l^{i,j} + 1/\bar{n}_i \delta_{ij})^2 \delta_{ll'}. \quad (32)$$

Therefore, in the general multibin case the full covariance matrix can be computed as:

$$\mathrm{Cov}(\omega^i(\theta_n)\omega^j(\theta_m)) = \frac{2}{f_{\mathrm{sky}}} \sum_l \left[\frac{2l+1}{(4\pi)^2} P_l(\cos\theta_n) P_l(\cos\theta_m) (C_l^{i,j} + 1/\bar{n}_i \delta_{ij})^2 \right] \quad (33)$$

with

$$C_l^{i,j} = \frac{2}{\pi} \int dk k^2 P(k) \Psi_l^i(k) \Psi_l^j(k). \quad (34)$$

In Fig 3 it is shown the cross-correlation angular power spectrum $C_l^{i,j}$ for the redshift shell $0.95 \leq z \leq 1.00$ with itself (autocorrelation) and its 3 nearest neighbors on one side. One can see that the cross-correlation for the nearest 2 shells is enough to capture the relevant effect. Hence in the following we will include the cross-correlation only with the neighboring 4 shells, 2 on each side.

V. ERROR FORECASTS FOR COSMOLOGICAL PARAMETERS

We will use the full shape of the angular correlation function $\omega(\theta)$ in our analysis to derive forecasts for the errors in the determination of cosmological parameters using a Fisher matrix approach.

The Fisher matrix approach approximates the full likelihood function of the parameters by a multivariate Gaussian distribution of the parameters [23,25]:

$$\mathcal{L}(\{p\}) \propto \exp\left[-\frac{1}{2} (p_\alpha - \bar{p}_\alpha) F_{\alpha\beta} (p_\beta - \bar{p}_\beta) \right], \quad (35)$$

that is, the Fisher matrix $F_{\alpha\beta}$ is the inverse of the covariance matrix for the parameters:

$$F_{\alpha\beta} = -\left[\frac{\partial^2 \log \mathcal{L}(\{p\})}{\partial p_\alpha \partial p_\beta} \right]_{\{\bar{p}\}} \quad (36)$$

where $\{\bar{p}\}$ denotes the best-fit parameters. We do not know *a priori* what the best-fit parameters are, since this involves a complicated search in the space with dimensions given by the total number of parameters. We will compare in the Appendix a few results from Fisher matrix with brute force computation of the likelihood function.

The most useful application of the Fisher matrix approach is to study *forecasts* of future experiments, determining the precision with which the parameters can be measured with respect to *fiducial* values. These fiducial values replace the unknown best-fit parameters.

The Fisher matrix in this case is given by

$$F_{\alpha\beta} = \frac{\partial \omega_{\mathrm{th}}^i(\theta^n, p)}{\partial p_\alpha} [C^{-1}]_{nm}^{ij} \frac{\partial \omega_{\mathrm{th}}^j(\theta^m, p)}{\partial p_\beta} + \frac{1}{2} \mathrm{Tr}\left[C^{-1} \frac{\partial C}{\partial p_\alpha} C^{-1} \frac{\partial C}{\partial p_\beta} \right] \quad (37)$$

where $C_{nm}^{ij} = \mathrm{Cov}(\omega^i(\theta_n)\omega^j(\theta_m))$ is the covariance matrix derived in the previous section and the derivatives are calculated at the fiducial set of parameters $\{\bar{p}\}$. In general the first term dominates over the second one [26] and our results will be obtained using only the first term. This is a conservative result and further below we will show that the second term indeed has a small impact on the forecast.

VI. RESULTS

We have divided a DES-like survey into 20 redshift shells with width $\Delta z = 0.05$ in the range $0.4 < z < 1.4$. We justify this value of Δz below. The angular binning varies with the redshift shell in order to select angles around the BAO peak position. The redshift and angular binnings are shown in Table (I) for the case of roughly $60 < r < 160 h^{-1}$ Mpc. The full correlation matrix in our case turns out to be a 445×445 matrix.

The C_l's were computed in a suite of C codes based on the free software Gnu Scientific Library [27]. The evaluation of the integrals of the rapidly oscillating spherical Bessel functions are particularly demanding. We compute the C_l's up to $l = 1000$ in order to obtain our results.

The reduced covariance matrix for one bin ($1.00 < z < 1.05$), defined by $R_{nm} = C_{nm}/\sqrt{C_{nn} C_{mm}}$ is shown in Fig. 4. In this case we used $f_{\mathrm{sky}} = 0.125$ and $\bar{n} = 15/\mathrm{arcmin}^2$. It can be seen that the errors in different angular bins are highly correlated resulting in a quasisingular covariance matrix. The magnitude of the first and second off-diagonal elements is typically 0.9 and 0.8. This is one of the major

TABLE I. Binning in redshift and angles (in degrees) for roughly $60 < r < 160h^{-1}$ Mpc

Redshift shell	Angular range	Bins	Bin width	Spatial scale
$0.40 < z < 0.45$	3–8	26	0.2	$60 < r < 160$
$0.45 < z < 0.50$	3–8	26	0.2	$67 < r < 180$
$0.50 < z < 0.55$	2.5–6.1	25	0.15	$61 < r < 149$
$0.55 < z < 0.60$	2.5–6.1	25	0.15	$66 < r < 162$
$0.60 < z < 0.65$	2–5.6	25	0.15	$57 < r < 159$
$0.65 < z < 0.70$	2–5.6	25	0.15	$61 < r < 170$
$0.70 < z < 0.75$	1.7–5.0	23	0.15	$55 < r < 162$
$0.75 < z < 0.80$	1.7–5.0	23	0.15	$58 < r < 171$
$0.80 < z < 0.85$	1.5–4.5	21	0.15	$54 < r < 161$
$0.85 < z < 0.90$	1.5–4.5	21	0.15	$56 < r < 169$
$0.90 < z < 0.95$	1.5–4.5	21	0.15	$59 < r < 177$
$0.95 < z < 1.00$	1.5–4.0	21	0.15	$61 < r < 183$
$1.00 < z < 1.05$	1.3–3.7	21	0.12	$55 < r < 157$
$1.05 < z < 1.10$	1.3–3.7	21	0.12	$57 < r < 163$
$1.10 < z < 1.15$	1.3–3.7	21	0.12	$59 < r < 168$
$1.15 < z < 1.20$	1.2–3.1	20	0.1	$56 < r < 145$
$1.20 < z < 1.25$	1.2–3.1	20	0.1	$58 < r < 150$
$1.25 < z < 1.30$	1.2–3.1	20	0.1	$60 < r < 154$
$1.30 < z < 1.35$	1.2–3.1	20	0.1	$61 < r < 158$
$1.35 < z < 1.40$	1.2–3.1	20	0.1	$63 < r < 162$

disadvantages of using the ACF to derive cosmological parameters.

In order to compute the Fisher matrix we invert the covariance matrix using singular value decomposition [28].

A. Redshift shell width and shot-noise

The narrower the redshift shell is, the larger signal is obtained for the angular correlation function, as illustrated in Fig. 5. However, one must be concerned with the impact of shot-noise on the forecast of cosmological parameters, which we analyze in this subsection.

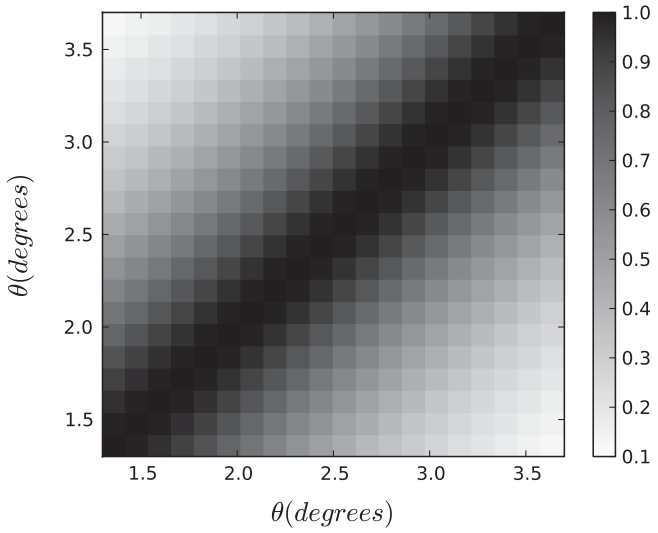

FIG. 4. Reduced covariance matrix for the bin $1.00 < z < 1.05$.

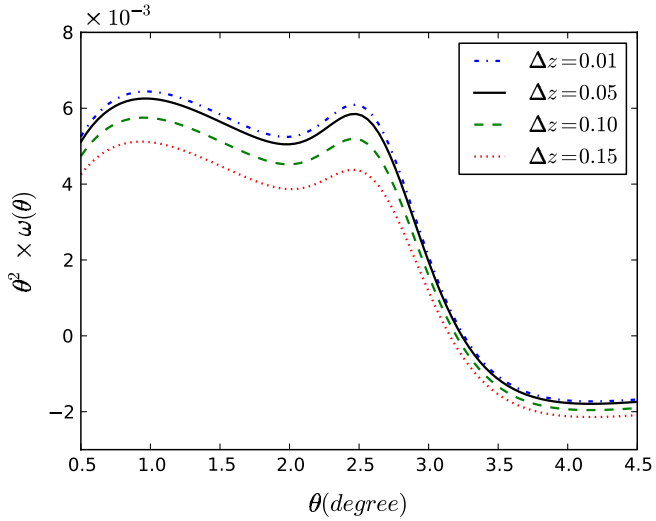

FIG. 5 (color online). Angular correlation function for a redshift bin centers at $z = 1.1$ for 4 different bin widths Δz.

In Fig. 6 we plot the 1σ error forecast on the determination of the equation of state w as a function of the shell width when marginalizing over the parameters $\Omega_{\rm cdm}$, σ_8 and bias, with the other parameters fixed at their fiducial values, and with a photo-z error given by $\sigma_z = 0.03(1+z)$. These forecasts were obtained for redshift shells centered at 3 mean redshift with different shell widths Δz. As expected, one can see that for very narrow redshift shells the shot-noise error becomes dominant even

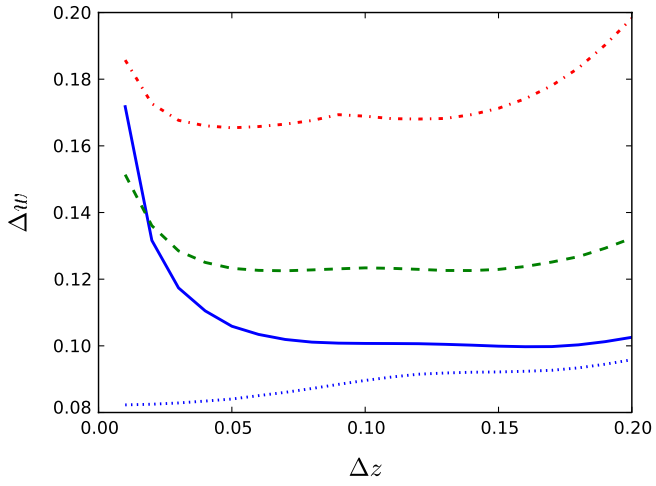

FIG. 6 (color online). The lines show the expected error on w as a function of the width of the shells centered at 3 mean redshifts. For all of them we are assuming $N_{\rm gal} = 300$ millions of galaxies and $\sigma_z = 0.03(1+z)$. The red dot-dashed line is centered at $z = 0.9$, the dashed green for $z = 1.1$ and the solid blue line for $z = 1.3$. The dotted blue line is the same as the last shell but now neglecting the contribution from the shot-noise.

for the DES expected number of galaxies, which we assume to be $N_{\rm gal} = 300$ million.

The best value for the shell width is around $\Delta z \sim 0.05$ (a similar result was found by [29], where they found that the best shell width for the redshift-space distortion parameter is ~0.07). The blue dotted line shows the error forecast on w when the shot-noise term is neglected. As expected if shot-noise is absent, the result improves as the width gets smaller because the angular correlation has more signal for thinner shells.

Another interesting feature of Fig. 6 is the flatness of the forecast error on w for $\Delta z \gtrsim 0.05$. One naively would expect that the constraint should degrade for very wide shells due to the washing out of the spatial correlation function when projecting on the sphere. However, as pointed out by Simpson *et al.* [21], the corresponding top-hat shell that simulates a true redshift distribution, denoted by $\Delta z_{\rm TH}$, can be obtained from the convolution of the top-hat shell in photometric redshift space Δz with the probability distribution for the photo-z error Eq. (12), which can be approximated by

$$\Delta z_{\rm TH} = \sqrt{\Delta z^2 + 12\sigma_z^2}. \tag{38}$$

From this relation we find for $\Delta z = 0.01$, 0.05, 0.10 and 0.15 the following top-hat values for the shell at $z = 1.1$ (green dashed line in Fig. 6), respectively: 0.219, 0.224, 0.240 and 0.265. Therefore, only for very wide redshift shells the true (spectroscopic) top-hat shell will have an impact in the cosmological parameters due to projection effects compared to very thin shells. Hence in what follows we set $\Delta z = 0.05$ through the entire redshift range.

B. Forecasts from the ACF

The sensitivity to the cosmological parameters for each shell increases with redshift, as exemplified in Fig. 7, where we show the errors in the equation of state obtained from each shell independently. This can also be seen in Fig. 8, where we show the forecasts on the equation of state w and the dark matter density $\Omega_{\rm cdm}$ obtained from 3 independent redshift shells, $0.40 < z < 0.45$, $0.85 < z < 0.90$ and $1.35 < z < 1.40$. We have marginalized over σ_8 and bias (we allow for a free bias parameter for each shell) but the other parameters are held at their fiducial values. One notices that the forecasts are better for shells at larger redshifts and that the ellipses rotate slightly from one shell to the next, a behavior which helps to break some of the degeneracies. The forecast errors are $\sigma_w = 0.071$ and $\sigma_{\Omega_{\rm cdm}} = 0.036$.

We also checked the robustness of this result if the other parameters are marginalized instead of fixed to their fiducial values. This is shown in Fig. 9, where the previous result with all parameters other than $\Omega_{\rm cdm}$ and w fixed at their fiducial values is shown in the solid ellipse. As expected, marginalizing over all other parameters without

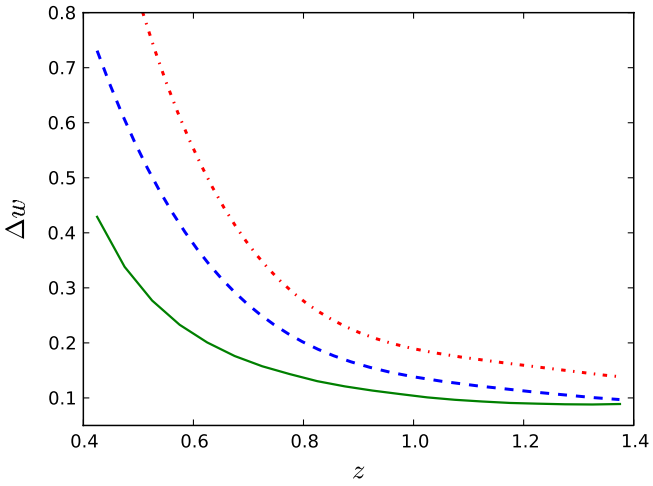

FIG. 7 (color online). Forecasts for 1-σ errors on the equation of state w as a function of redshift with marginalized bias, σ_8 and $\Omega_{\rm cdm}$. Optimistic case with $\delta_\sigma = 0.03$ and $20 < r < 200h^{-1}$ Mpc (solid green line), fiducial case with $\delta_\sigma = 0.03$ and $60 < r < 160h^{-1}$ Mpc (dashed blue line) and conservative case $\delta_\sigma = 0.05$ and $60 < r < 160h^{-1}$ Mpc (dot-dashed red line).

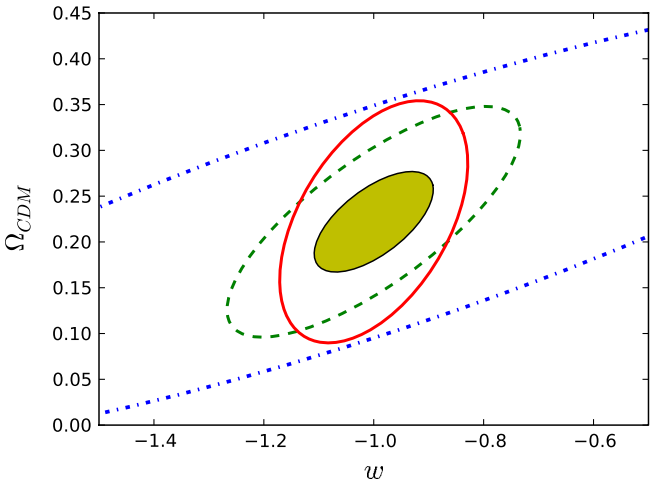

FIG. 8 (color online). Forecasts for $\Omega_{\rm cdm}$ and w from the angular correlation function of three redshift shells, $0.40 < z < 0.45$ (blue dot-dashed line),$0.85 < z < 0.90$ (green dashed line) and $1.35 < z < 1.40$ (red solid line). The yellow ellipse is the result of combining the 3 shells.

any priors (dot-dashed ellipse) degrades the forecasts significantly. The errors on the parameters without any priors are $\sigma_w = 0.34$, $\sigma_{\Omega_{\rm cdm}} = 0.047$, $\sigma_{\Omega_b} = 0.022$, $\sigma_h = 0.26$, $\sigma_{n_s} = 0.31$ and $\sigma_{\sigma_8} = 0.77$. However, introducing priors only on h (from HST) and Ω_b from WMAP7 (dashed ellipse) again reduces the errors of the forecasts.

As explained above, our results will be conservative since we are neglecting an extra term in the Fisher matrix. To assess the small impact of the neglected term, we plot in Fig. 10 the analysis for all redshift bins without

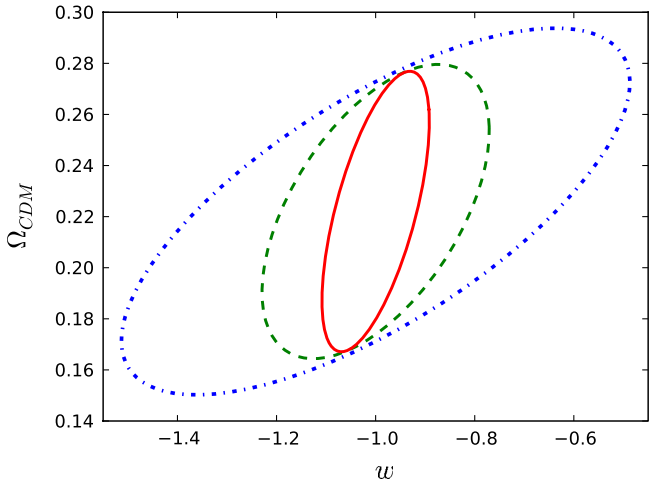

FIG. 9 (color online). Forecasts for $\Omega_{\rm cdm}$ and w from the angular correlation function of five redshift shells. The red solid ellipse is the result with all parameters fixed at their fiducial values; blue dot-dashed ellipse is the result with all parameters marginalized without priors; green dashed ellipse is the result with priors on h and Ω_b.

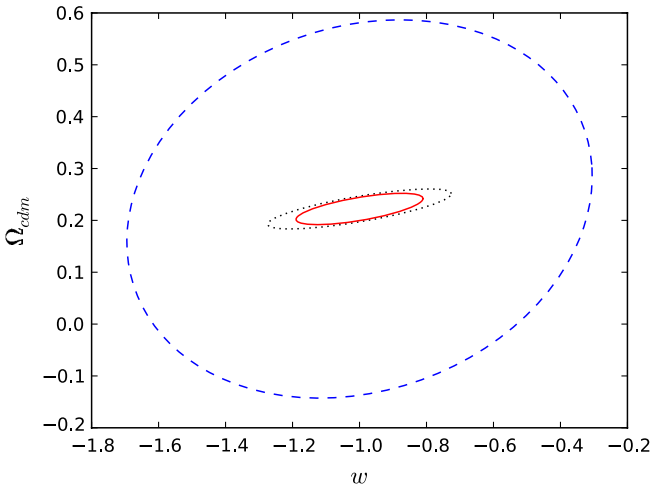

FIG. 10 (color online). Forecasts for $\Omega_{\rm cdm}$ and w from the angular correlation function for all redshift shells without correlation among shells. Contribution from the neglected term (dashed line), contribution from the dominant term (dotted line) and result from both terms (solid line).

correlations among bins with and without the contribution from the neglected term. We see that, as expected, including the second term leads to a slightly more restrictive forecast.

We now proceed to our complete analysis. We consider 26 parameters, namely n_s, σ_8, h, Ω_b, $\Omega_{\rm cdm}$, w, b_1, $b_2, \cdots, b_{20}$, where b_i are the bias for the ith redshift shell. We include correlations for the adjacent 2 redshift bins, i.e. for each bin we take correlations with 4 bins. In order to show the impact of including these correlations we show in Fig. 11 the 1σ constraint on $\Omega_{\rm cdm}$ and w with all other parameters marginalized without priors. As expected, it can be seen that the error is underestimated when the correlations are not taken into account.

In Fig. 12 we plot the 1σ ellipses for the parameters n_s, h, Ω_b, $\Omega_{\rm cdm}$ and w, marginalizing over σ_8 and bias. When two of these parameters are plotted all the others are marginalized with no priors. We study three scenarios: optimistic ($20 < r < 200h^{-1}$ Mpc and $\delta_\sigma = 0.03$), fiducial ($60 < r < 160h^{-1}$ Mpc and $\delta_\sigma = 0.03$) and pessimistic ($60 < r < 160h^{-1}$ Mpc and $\delta_\sigma = 0.05$). One can see that a larger photo-z error degrades substantially the possible forecasts. This is expected since for larger photo-z errors the signal coming from the spatial correlation function becomes weaker. The forecast error for w goes from $\sim$0.3 with $\delta_\sigma = 0.03$ to $\sim$0.5 for $\delta_\sigma = 0.05$.

One can also notice from Fig. 12 that the constraint in w is not very sensitive to the scales probed. Nevertheless, the other parameters $\Omega_{\rm cdm}$, Ω_b, n_s and h are significantly dependent on the scales probed, especially Ω_b and n_s. This shows that those cosmological parameters change the ACF at all scales and not only around the BAO feature like w.

Finally we investigate the role of priors in the forecasts in Fig. 13. In particular, we use the HST prior on h [30] and WMAP7 priors from the acoustic scale l_A, the redshift of decoupling z_* and the shift parameter R (Table 10 of Komatsu *et al.* [18]) and also imposed *a prior* in n_s from WMAP7. The WMAP7 covariance matrix in l_A, z_* and R was then converted to our set of cosmological parameters using a method described in Mukherjee *et al.* [31] and Wang *et al.* [32].

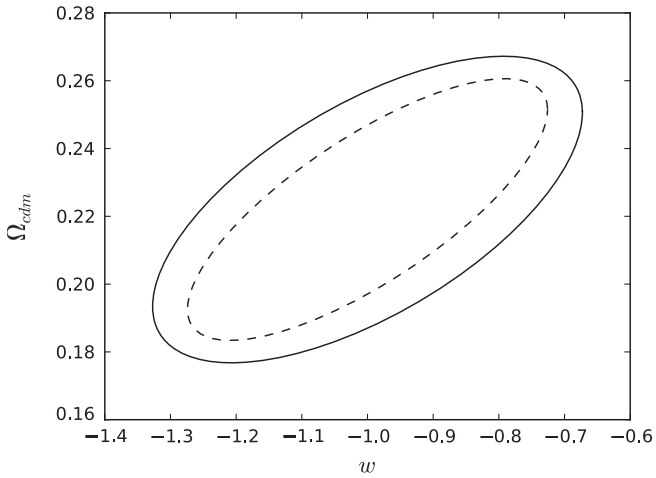

FIG. 11. Forecasts for $\Omega_{\rm cdm}$ and w from the angular correlation function with all redshift shells included. All other parameters are marginalized with no priors and $\delta_\sigma = 0.03$. Dashed line is the result with diagonal correlation matrix (only autocorrelations) and full line is the result taking into account next 2 neighbor bins.

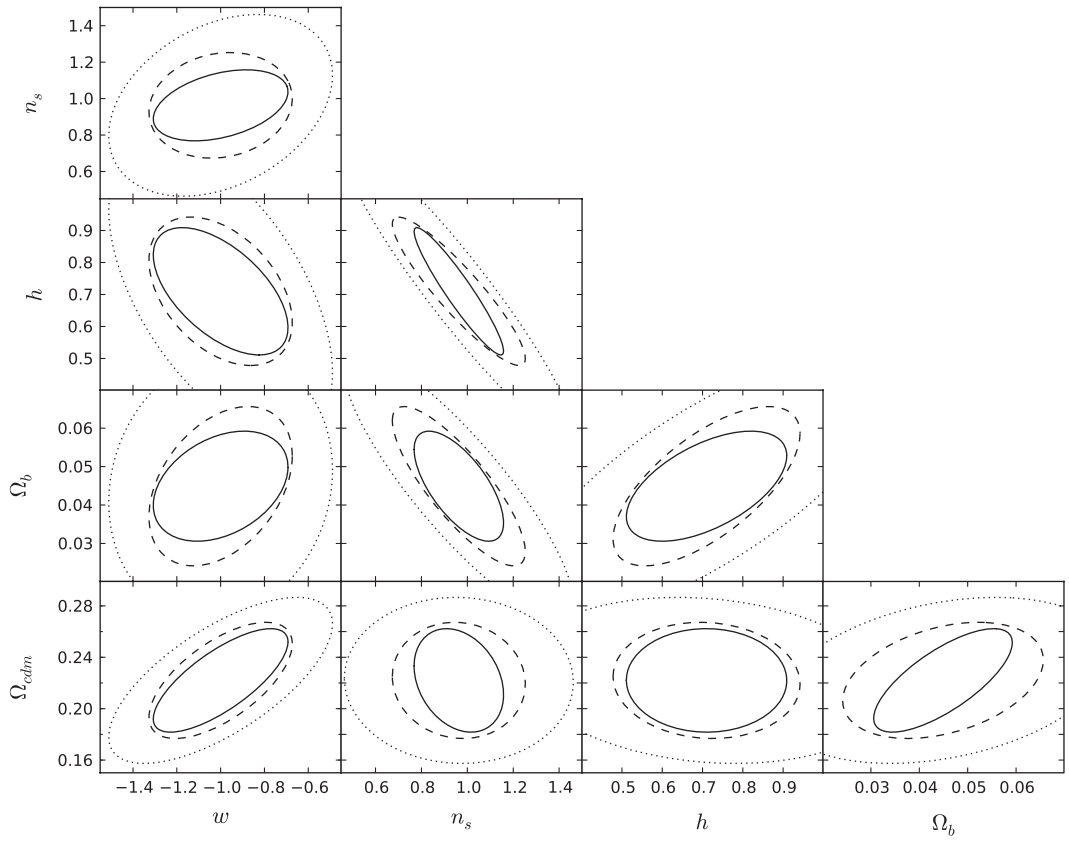

FIG. 12. 1σ forecasts for n_s, h, Ω_b, $\Omega_{\rm cdm}$ and w, marginalizing over σ_8 and bias, for three scenarios: optimistic (solid line) ($20 < r < 200$ Mpc and $\delta_\sigma = 0.03$), fiducial (dashed line) ($60 < r < 160$ Mpc and $\delta_\sigma = 0.03$) and pessimistic (dotted line) ($60 < r < 160$ Mpc and $\delta_\sigma = 0.05$).

We find the 1-σ marginalized error on a given cosmological parameter p via

$$\sigma_p = \sqrt{[F^{-1}]_{pp}}. \tag{39}$$

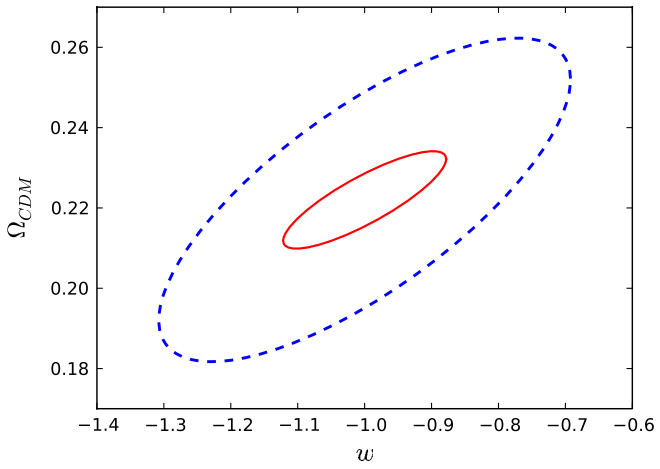

FIG. 13 (color online). $\Omega_{\rm cdm} \times w$ 1σ forecasts in the optimistic scenario in the case of no priors (dashed line), and adding priors from WMAP7 and HST as explained in the text (solid line).

In our optimistic best case scenario one would be able to obtain $\sigma_w = 0.2$ and $\sigma_{\Omega_{\rm cdm}} = 0.03$ without priors and $\sigma_w = 0.08$ and $\sigma_{\Omega_{\rm cdm}} = 0.009$ with priors.

C. Impact of fiducial bias

The analysis presented until now was performed assuming a fiducial galaxy bias $b = 2$ for each redshift shell. This is the usual value for catalogues of luminous red galaxies (LRG). However, it is more likely that the galaxy bias will have lower values for the complete galaxy set. In this subsection we show how our results change if the galaxies in the catalog are assumed to be unbiased on average with $b = 1$, as done in [29].

As shown in [26], the statistical reach of a survey can be assessed from its effective volume, which is proportional to b^2. Hence, it is expected that the constrain on the cosmological parameters will degrade if the fiducial bias decreases. In order to evaluate the impact of the bias on the cosmological parameters, we have performed the Fisher matrix analysis with a fiducial bias $b = 1$ and compared to the results arising from $b = 2$.

In Fig. 14, we show the forecast for our optimistic scenario. In this case the constrain on w degrades by 17%, with respect to $b = 2$, and the expected constrain

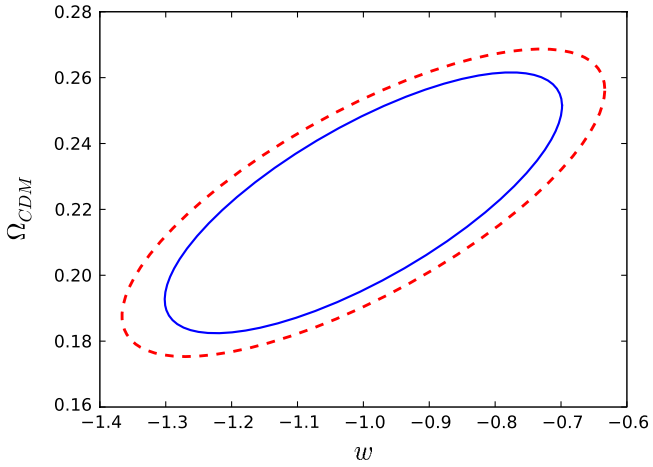

FIG. 14 (color online). 1σ forecats for w and $\Omega_{\rm cdm}$ for the optimistic scenario with two fiducial bias: $b = 2$ (blue solid line) and $b = 1$ (red dashed line).

on w is $\sigma_w = 0.24$. This analysis shows that the fiducial galaxy bias does have a minor impact in the dark energy constraints.

VII. SUMMARY AND CONCLUSIONS

In this paper we have investigated the forecasts on cosmological parameters that can be obtained from a study of the full shape of the 2-point angular correlation function that will be measured by future large-scale photometric surveys, such as the Dark Energy Survey project. The angular correlation function was modeled taking into account redshift-space distortion, nonlinear corrections to the power spectrum, bias and Gaussian photo-z errors. After a proper binning in angle and redshift, the Fisher information matrix was constructed from a covariance matrix that includes correlation of a given redshift bin with the 4 nearest bins. We considered 26 parameters: n_s, σ_8, h, Ω_b, $\Omega_{\rm cdm}$, w, b_1, $b_2, \cdots, b_{20}$ with different bias for each shell.

We used the 26×26 Fisher matrix to obtain 1σ ellipses for the cosmological parameters around the adopted fiducial values obtained from the central values of WMAP7 measurements. In all our results we marginalize over the bias parameters and σ_8. After showing results for several combinations of parameters in Fig. 12, we concentrate on forecasts on the $\Omega_{\rm cdm} \times w$ plane. We have shown the improvements of using priors from other experiments such as WMAP7 and HST in comparison to a simple marginalization of parameters. Finally, we showed that the effect of neglecting the second term in the Fisher matrix Eq. (38) is in fact unimportant, as usually assumed in the literature [26].

In the Appendix we make a comparison between the Fisher matrix approximated methodology and a full likelihood search in parameter space which validates the Fisher matrix approach.

We find that under these assumptions the Dark Energy Survey should be able to constrain the dark energy equation of state parameter w and the cold dark matter density $\Omega_{\rm cdm}$ with a precision of 20% and 13%, respectively, from the full shape of the angular correlation function alone. When combined with priors from other observations the precision in the determination of these parameters increase to 8% and 4%, respectively.

For comparison, the WiggleZ Dark Energy Survey has recently obtained $w = -1.6^{+0.6}_{-0.7}$ from BAO data alone, which is improved to $w = -0.982^{+0.154}_{-0.184}$ when WMAP7 distance priors are included [33], which amounts to a precision of approximately 40% (15% with priors). Therefore, measurements of the angular correlation function from a DES-like survey will improve the constraint on w by a factor of $\mathcal{O}(2)$, in the case where only galaxy clustering measurements are used. It is also expected that the constraints we have found will improve as the redshift range, area and number of galaxies improve with future photometric surveys.

In conclusion, our results indicate that an analysis of the full shape of the 2-point angular correlation function can in fact bring an important contribution to the determination of cosmological parameters in future photometric redshift surveys. This contribution is of course complementary to the other observables that will be used in a DES-like survey, including cluster number counts, shear from weak lensing and distances from SNIa. One challenge that remains is to combine our results with these other probes in a consistent manner, including the proper correlations.

ACKNOWLEDGMENTS

We wish to thank Filipe Abdalla, Martin Crocce, Enrique Gaztañaga, Mariana Penna-Lima, Ashley Ross, Sandro Vitenti, the DES-Brazil Collaboration and the DES LSS-WG for useful comments. We especially thank Marcos Lima for a careful reading of this manuscript and valuable suggestions. This research was carried out with the support of the Laboratório Interinstitucional de e- Astronomia (LIneA) operated jointly by the Centro Brasileiro de Pesquisas Físicas (CBPF), the Laboratório Nacional de Computação Científica (LNCC) and the Observatório Nacional (ON) and funded by the Ministério de Ciência e Tecnologia (MCT). F. S. is supported by a Ph.D. grant from CAPES. F. dS. acknowledges financial support from the CNPq (DTI grant 381.392/09-0 associated with the PCI/MCT/ON Program). The work of R. R. is supported by Fapesp and CNPq. L. N. dC. acknowledges CNPq grants 476277/2006 and 304.202/2008-8, FAPERJ grants E-26/102.358/2009 and E-26/110.564/2010, and FINEP grants 01.06.0383.00 and 01.09.0298.00. M. M. is partially supported by CNPq (grants 312876/2009-2, 486138/2007-0, and 312425/2006-6) and FAPERJ (grant E-26/171.206/2006).

TABLE II. Grid parameters.

Parameter	Lower bound	Upper bound	$N_{\rm grid}$
w	-2.0	0.0	80
$\Omega_{\rm cdm}$	0.05	0.55	100
σ_8	0.1	2.1	100
b	0.05	5.55	100

APPENDIX

In this Appendix we check the reliability of the Fisher matrix forecast by computing the likelihood function on a grid of values for the parameters. Here we concentrate on a single redshift shell, $0.70 \leq z \leq 0.75$, and examine 4 free parameters, namely w, $\Omega_{\rm cdm}$, b and σ_8, with a grid constructed around their fiducial values, see Table (II). Once the grid is created it is fairly easy to search the likelihood function and compare it with the Fisher matrix approach.

In Fig. 15 we compare the likelihood for w when marginalizing over the other 3 parameters. In this case, the Fisher matrix prediction is in good agreement with the results from the grid. The Fisher matrix forecasts an error of $\sigma_w(\text{fisher}) = 0.23$, exactly the same value obtained from the grid. It is interesting to note that the true distribution has a small skewness towards higher values, showing that it is not a perfect Gaussian distribution, but in overall both distributions are in fair agreement.

For $\Omega_{\rm cdm}$ we find the same trend as for w, but here the difference between Fisher matrix and the grid likelihood is slightly larger, as shown in Fig. 16. In this case the $\Omega_{\rm cdm}$ has a more pronounced non-gaussianity, with a skewness towards higher values. However, the prediction for the standard deviation from Fisher matrix is again in fairly good agreement with the grid, with $\sigma_{\rm cdm}(\text{fisher}) = 0.088$ and $\sigma_{\rm cdm}(\text{grid}) = 0.064$. In this case the Fisher matrix method overestimates the error on $\Omega_{\rm cdm}$ due to the non-gaussianity of the likelihood.

This simple comparison shows that the Fisher matrix gives reliable predictions for the forecasts of the cosmological parameters w and $\Omega_{\rm cdm}$ that we obtained in this work.

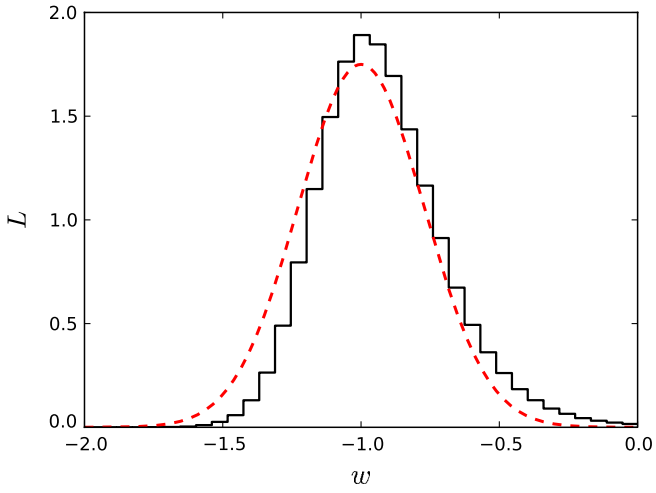

FIG. 15 (color online). The actual distribution for w estimated with the grid when the other 3 free parameters are marginalized (solid line) compared with the Gaussian distribution predicted by the Fisher matrix (dashed line).

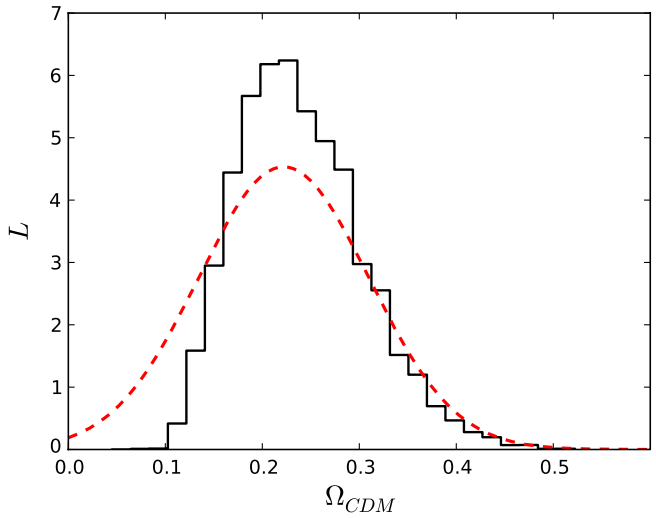

FIG. 16 (color online). The actual distribution for $\Omega_{\rm cdm}$ estimated with the grid when the other 3 free parameters are marginalized (solid line) compared with the Gaussian distribution predicted by the Fisher matrix (dashed line).

[1] M. Colless *et al.*, Mon. Not. R. Astron. Soc. **328**, 1039 (2001).
[2] D. G. York *et al.*, Astron. J. **120**, 1579 (2000).
[3] D. J. Eisenstein *et al.*, Astrophys. J. **633**, 560 (2005).
[4] A. Collister *et al.*, Mon. Not. R. Astron. Soc. **375**, 68 (2007).
[5] S. A. Thomas, F. B. Abdalla, and O. Lahav, arXiv:1011.2448.
[6] U. Sawangwit, T. Shanks, F. B. Abdalla, R. D. Cannon, S. M. Croom, A. C. Edge, N. P. Ross, and D. A. Wake, Mon. Not. R. Astron. Soc. **416**, 3033 (2011).
[7] The Dark Energy Survey Collaboration White Paper, arXiv:astro-ph/0510346.
[8] E. Sánchez *et al.*, Mon. Not. R. Astron. Soc. **411**, 277 (2011).
[9] A. J. S. Hamilton, Astrophys. J. **385**, L5 (1992).
[10] T. Matsubara, Astrophys. J. **537**, L77 (2000).

[11] C. M. Baugh and G. Efstathiou, Mon. Not. R. Astron. Soc. **265**, 145 (1993).
[12] L. Sun *et al.*, Astrophys. J. **699**, 958 (2009).
[13] M. Crocce, A. Cabre, and E. Gaztañaga, Mon. Not. R. Astron. Soc. **414**, 329 (2011).
[14] A. P. Hearin, A. R. Zentner, Z. Ma, and D. Huterer, Astrophys. J. **720**, 1351 (2010).
[15] Z. Ma, W. Hu, and D. Huterer, Astrophys. J. **636**, 21 (2006).
[16] A. J. Ross *et al.*, arXiv:1105.2320.
[17] M. Crocce and R. Scoccimarro, Phys. Rev. D **77**, 023533 (2008).
[18] E. Komatsu *et al.* (WMAP Collaboration), Astrophys. J. Suppl. Ser. **192**, 18 (2011).
[19] C. Blake, A. Collister, S. Bridle, and O. Lahav, Mon. Not. R. Astron. Soc. **374**, 1527 (2007).
[20] T. Okumura, T. Matsubara, D. J. Eisenstein, I. Kayo, C. Hikage, A. S. Szalay, and D. P. Schneider, Astrophys. J. **676**, 889 (2008).
[21] F. Simpson, J. A. Peacock, and P. Simon, Phys. Rev. D **79**, 063508 (2009).
[22] J. D. Cohn, New Astron. Rev. **11**, 226 (2006).
[23] See, *e.g.* chapter 11 in S. Dodelson, *Modern Cosmology* (Academic Press, San Diego, 2003).
[24] N. Padmanabhan *et al.*, Mon. Not. R. Astron. Soc. **378**, 852 (2007).
[25] M. Tegmark, A. N. Taylor, and A. F. Heavens, Astrophys. J. **480**, 22 (1997).
[26] M. Tegmark, Phys. Rev. Lett. **79**, 3806 (1997).
[27] Gnu Scientific Library, http://www.gnu.org/gsl.
[28] W. H. Press, S. A. Teukolsky, W. T. Vetterling, and B. P. Flannery, *Numerical Recipes: The Art of Scientific Computing* (Cambridge University Press, Cambridge, England, 2007), 3rd ed..
[29] A. J Ross, W. J Percival, M. Crocce, A. Cabre, and E. Gaztanaga, arXiv:1102.0968.
[30] A. G. Riess *et al.*, Astrophys. J. **699**, 539 (2009).
[31] P. Mukherjee, M. Kunz, D. Parkinson, and Y. Wang, Phys. Rev. D **78**, 083529 (2008).
[32] Y. Wang *et al.*, Mon. Not. R. Astron. Soc. **409**, 737 (2010).
[33] C. Blake *et al.*, arXiv:1105.2862.